



**HAL**  
open science

## Study of stator core-end packets under the action of two incident fluxes -Real scale model

Gilles Vogt, Raphael Romary, Guillaume Parent, Valentin Costan

► **To cite this version:**

Gilles Vogt, Raphael Romary, Guillaume Parent, Valentin Costan. Study of stator core-end packets under the action of two incident fluxes -Real scale model. IECON 2012 - 38th Annual Conference of IEEE Industrial Electronics, Oct 2012, Montreal, QC, Canada. pp.2043-2048, 10.1109/IECON.2012.6388744 . hal-04260743

**HAL Id: hal-04260743**

**<https://hal.science/hal-04260743>**

Submitted on 26 Oct 2023

**HAL** is a multi-disciplinary open access archive for the deposit and dissemination of scientific research documents, whether they are published or not. The documents may come from teaching and research institutions in France or abroad, or from public or private research centers.

L'archive ouverte pluridisciplinaire **HAL**, est destinée au dépôt et à la diffusion de documents scientifiques de niveau recherche, publiés ou non, émanant des établissements d'enseignement et de recherche français ou étrangers, des laboratoires publics ou privés.

# Study of stator core-end packets under the action of two incident fluxes – Real scale model

Gilles Vogt<sup>\*†</sup>, Raphaël Romary<sup>†</sup>, Guillaume Parent<sup>†</sup> and Valentin Costan<sup>\*</sup>

<sup>\*</sup> Électricité de France (EDF) R&D, 92141 Clamart, France

<sup>†</sup> Univ. Lille Nord de France, F-59000 Lille, France - UArtois, LSEE, F-62400 Béthune, France

**Abstract**—This paper describes an experimental procedure for characterization of electromagnetic phenomena that occur in the end regions of large turbo-generators. The test bench contains a stack of steel laminations from a 900MW turbo-generator stator and two exciting circuits in order to combine a transverse magnetic flux with the in-plane flux. The theoretical and experimental results will be analyzed with a view to examine the influence of transverse flux on losses.

**Index Terms**—Turbo-generator, real scale model, 3D finite element method, transverse field, perpendicular flux, core end, eddy currents, stray losses.

## I. INTRODUCTION

Stator magnetic circuit of large power-generators in electrical power-plants are subjected to electrical, thermal and vibratory stresses which causes aging and deterioration. Especially, the stator front ends are severely stressed due to the presence of the stray magnetic field induced by the current in the end windings and in the rotating end connections of the rotor. Indeed, this magnetic field has an axial component which penetrates perpendicularly in the front parts laminations. This transverse magnetic field induces in plane eddy currents in the first laminations, leading to extra losses and overheating. The thermal stress causes fast aging of insulation between laminations at the end part of the stator, which can induce breakdown of the insulation, possibly generating stator core faults.

The electromagnetic field in these parts of the machine is fully three-dimensional. Until now, finite element simulations that compute that field are mainly based on simplified two-dimensional models [1] or simplified 3D models (that does not allow the analysis of eddy currents, or based on simplified geometry) [2]. Moreover, experimental analysis is uneasy because it requires an experimental bench that represents a real stator, or at least a piece of real stator, what is rather unusual.

This paper presents an analysis based on a device made of stator laminations of a large turbo-generator. The particularity of the device concerns the double excitation of the laminations that bring the main flux density longitudinally but also a transverse magnetic field. The both fields can be adjusted separately in amplitude and in phase. In this way it is possible to reproduce the behavior of the laminations versus the active and reactive power delivered by the power generator.

The study will combine a finite element simulation and an experimental analysis. The finite element analysis is based on

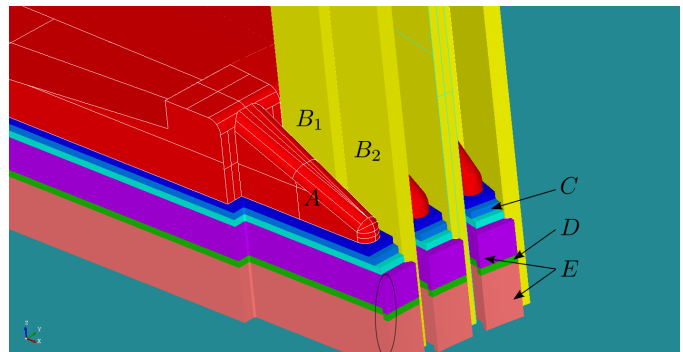


Figure 1. Model of the end region of the stator core of a 125 MW turbo-generator as an example of a stepped core. Zoom on the first steps around the teeth (only half a segment is drawn). It is a not-shielded stator, and its fingers are drawn in red (A), the stator bars in yellow (B<sub>1</sub> and B<sub>2</sub>), the stepped core end in shaded blues (C), the cooling ducts in green (D) and the full segments in purple and pink (E) that comprise notches (circled in the figure).

a 3D harmonic model that takes into account a homogenized anisotropic conducting block for the stator laminations; this method will be shortly explained and tested.

The effect of the transverse magnetic flux will be studied in terms of additional iron losses at a given main in-plane flux. Two results are presented in this paper: the influence of a passive additional magnetic path equivalent to a strong air-gap fringing, and the evolution of the losses in the tooth with regard to the incoming transverse flux density.

## II. OBJECTIVES AND DESIGN

### A. Background and objectives

In the end region of large turbo-generators, the magnetic field includes an axial component which comes mainly from the air-gap fringing across the core end and from the stator and rotor end-winding currents [3]. The effects of the axial-flux are reduced by introducing a stepped core end (see in figure 1), a core end flux shield or by slit cuts on the tooth. However, it still induces eddy currents and inter-lamination voltages [4] that might damage the stator core by breaking the insulation between laminations and thus providing a path for a default current.

Eddy currents from axial flux increase definitely the global stray losses, but the heating is indeed localized in some areas, e.g. the corners at the far end of stator slots [5]. Both experiments and simulations are thus important to determinate

the critical areas. The operating conditions also have a major influence on the magnitude of axial flux: it is well known that during leading power factor operations, the heat may be critical; and the worst case remains the pole-slip [6].

Experimental measurements were made on stator core end of some large turbo-generator [7], [8], but instrumenting a real turbo-generator generator remains complicated, and monitoring at operating conditions is usually not possible. These difficulties justify the use of simulations and simplified devices.

The experimental device designed in the present paper aims at studying the behavior of the magnetic flux in the end region of the turbo-generator. This study focuses on the combination of fluxes within the teeth, and the induced losses, function of the phase shift between both fluxes and magnetic flux density level.

### B. Specifications

The scale model aims at simulating the behavior of the fluxes in the end region of large turbo-generators; thus it must combine two normal incoming fluxes. The first one is the “main” flux of the turbo-generator, circulating within the plane of lamination, and the second one is the leakage flux, incoming across the sheets of the magnetic core.

The specifications of the scale model are therefore:

- Being a good approximation of the phenomena that occur in the end region of large turbo-generators;
- Generating a high magnetic flux in the tooth (in order to get the highest saturation as possible) within the plane of lamination called hereafter “lengthwise flux”;
- Generating a magnetic flux perpendicular to the sheets upon the tooth, called “transverse flux”;
- Controlling the phase difference between both fluxes in order to reproduce the operating conditions (*i.e.* lagging/leading mode);
- Measuring the flux penetration inside the stator sheets stack, measuring losses function of phase shift between incoming fluxes.

### C. Design

The final design is depicted in the figure 2. Several choices have been made in order to fulfill the specifications.

1) *Test core sheets (C in figure 2)*: The chosen testing sample is an actual part of a 900 MW turbo-generator core (real scale). On the 900 MW turbo-generator, the stator magnetic core is made up of stacked laminations; each layer is divided into 18 segments of 3 teeth (the stator has 54 slots). The butt joints between laminations are staggered from layers to layers; the shift angle between adjacent laminations is equivalent to one tooth. That is why the angular aperture of one sample sheet equates to one third of the actual segments (*i.e.* one tooth only): a stack of full segments without staggering would not be more accurate.

This design allows besides to focus the lengthwise flux into one single tooth, increasing the flux density. Using a single tooth on a full three-teeth segment would neither improve the

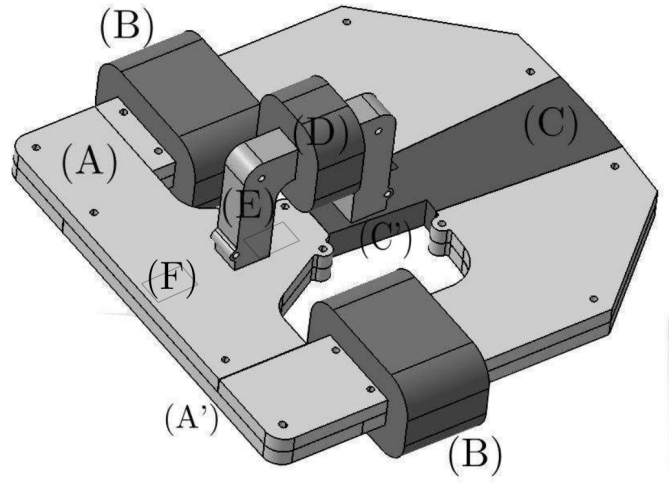


Figure 2. Final design of the scale model. (A): lengthwise exciter’s frame and (A’): butt-lap (sketched with two layers of over-thick sheets); (B): lengthwise exciter’s windings; (C): 900 MW sheet samples and (C’): stator tooth; (D): transverse exciter’s winding; (E): transverse exciter’s frame.

accuracy since the two adjacent teeth would not carry any magnetic flux (unlike what actually occurs).

Moreover, in the end region of turbo-generators the teeth are shortened (in order to obtain a stepped core end as shown in the figure 1), thus the notches used to maintain the wedges in this area do not appear in the presented device. Finally, some teeth are designed with slits cut in the radial direction, but this is neglected in the current study. The samples may include this in further studies.

The sample sheets are made of a grain oriented electrical steel (thickness 0.35 mm). The direction of lamination is crosswise to the tooth.

2) *Exciter frame (A in figure 2)*: The lengthwise flux, which flows within the plane of laminations, is generated by two windings on a symmetric exciter frame, as shown in the figure 2. The two windings (B) work in phase, producing two symmetric fluxes that move back through the tooth; however an asymmetric mode would be easy to implement afterward.

The transverse flux is generated by a second frame in “U” shape (E). It is mobile, so the incoming area may be adjusted upon the tooth. The air-gaps between the exciter frame (A) and the sample (C) may be widened or narrowed in order to fine-tune the global reluctance of the exciter.

The frames themselves are made of a stack of 180 laminations (M270-0.35). The lengthwise frame is divided in 3 parts with butt-lap to reduce the reluctance of the frame, the transverse frame is made of one part.

3) *Phase shift between fluxes*: An asynchronous machine with a wound rotor is used as transformer to feed the transverse winding. This way, the phase angle between lengthwise and transverse fluxes depends directly on the angular position of the rotor (which is fixed and adjustable using a worm screw).

4) *Windings sizing*: The number of turns must be determined beforehand: the required current to impose a flux decreases when the number of turns increases, however the re-

quired voltage rises. Depending on the chosen power supply's characteristics, the best compromise voltage/current must be evaluated: a model based on reluctance network will be used.

5) *Reluctance network*: A simple (linear) reluctance network has been drawn, as shown in the figure 3. The two branches (( $\alpha$ ) and ( $\alpha'$ )) modeling the lengthwise frame are symmetric: they consist of one magnetomotive force  $n_l i_l$  (M.M.F. that represents the winding) and one reluctance  $R_1$ . This reluctance  $R_1$  includes the reluctances from the magnetic frame, the butt-lap joint (which equates to an air gap of  $\sim 0.1$  mm [9]), the long air-gap and a part of the sample (depending on the position of the transverse frame). The branch ( $\beta$ ) corresponds to the transverse frame: the M.M.F.  $n_t i_t$  and one reluctance  $R_3$  that includes the two air-gaps reluctances and the magnetic frame's reluctance. Finally, the branch ( $\gamma$ ) (reluctance  $R_2$ ) represents one part of the sample (complementary to the  $\alpha$ 's part), the tooth air-gap and the part of the lengthwise frame that faces the tooth (triangular-shaped).

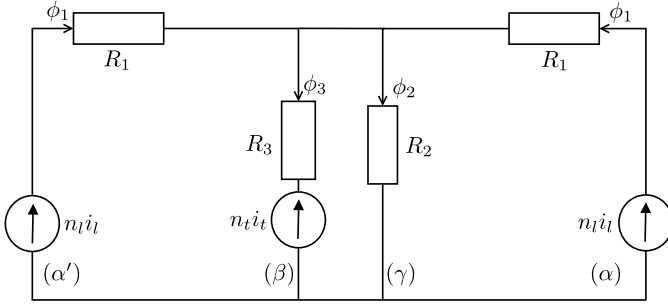


Figure 3. Reluctance network. ( $\alpha$ ) and ( $\alpha'$ ): lengthwise frame and windings; ( $\beta$ ): transverse frame and winding; ( $\gamma$ ): central branch including the tooth.

The saturation of the material is taken into account through the adaptation of the magnetic permeability. In the areas where the flux density is expected to be high (confirmed by FEM simulation), such as the tooth, the permeability is lowered. The relative permeability of the lengthwise frame is 4000, while the tooth's one is only 500 (which is coherent with an induction of  $\sim 1.7$  T).

The reluctance of a circuit  $[AB]$  is calculated using the following formula (1), where  $l$  is the curvilinear abscissa,  $S$  and  $\mu$  the current section and permeability:

$$R = \int_A^B \frac{dl}{\mu(l) \cdot S(l)} \quad (1)$$

Of course, in the case where the permeability and section are constant, the formula becomes  $R = l_{AB}/\mu \cdot S$ .

This leads to the electrical equations that describes the behavior of the system. The results are shown in the table I which points out that the reluctance frame provides an alternative path for the flux. Adjusting the air-gaps accordingly (e.g. by increasing the transverse air-gaps) will allow to control this path. Nevertheless, the reluctance network highlighted this intrinsic restriction of the device.

Portion	Value ( $H^{-1}$ )	Reluctance	Value ( $H^{-1}$ )
Tooth (total)	$10.6 \cdot 10^4$	$R_1$	$18.1 \cdot 10^4$
Tooth air-gap	$2.1 \cdot 10^4$	$R_2$	$6.7 \cdot 10^4$
Long air-gap	$2.1 \cdot 10^4$	$R_3$	$11.6 \cdot 10^4$
Transverse air-gap	$3.2 \cdot 10^4$		
Transverse frame	$4.2 \cdot 10^4$		
Lengthwise frame	$2.2 \cdot 10^4$		

Table I  
RELUCTANCES OF THE MAIN PARTS OF THE SCALE MODEL (cf. FIGURE 3).

The lengthwise windings are sized by shutting down the transverse winding, and *vice versa*. For instance, the global magnetic equation for the lengthwise case is:

$$\phi_2 \left( R_2 + \frac{R_2 + R_3}{2R_3} R_1 \right) = n_l i_l \quad (2)$$

Where  $n_l$  is the number of turns and  $i_l$  the current in the lengthwise windings. In order to gauge the number of turns, a flux density set-point  $B_{obj}$  in the tooth is chosen, leading to the system (4).

$$e_l = -n \frac{\partial \phi_l}{\partial t} = -n \frac{\partial \int_{S_l} \vec{B}_{obj} \cdot d\vec{S}}{\partial t} \quad (3)$$

$$\begin{cases} i_l &= \frac{1}{n_l} \cdot 629 \cdot B_{obj} \\ e_l &= 0.94 \cdot n_l \cdot B_{obj} \end{cases} \quad (4)$$

Where  $e_l$  is the voltage across the lengthwise winding terminals and  $\phi_l$  the magnetic flux through the winding section.

The flux density objective level  $B_{obj}$  is set to  $1.7$  T, and it appears that  $e_l = 240$  V and  $i_l = 7$  A (for each winding) are enough with  $n_l = 150$  turns. The same analysis (with  $B_{obj} = 1$  T) for the transverse exciter leads to the same number of turns ( $n_t = 150$ ), but with much lower electric levels ( $i_t = 5$  A and  $e_t = 140$  V).

### III. FEM SIMULATIONS

The finite element model of the experimental apparatus is used to characterize the flux density distribution inside the stator packets imposing different values of the currents through the exciting circuits.

#### A. Code\_Carmel3D

The FEM (Finite Elements Method) simulations are run with code\_Carmel3D. This software is based on Whitney's elements and is developed by the LAMEL ("Laboratoire de Modélisation du Matériel Electrique", common laboratory between EDF R&D and L2EP).

#### B. Mesh of the experimental apparatus

The geometric model is based on the true geometric shape of the scale model, including screw holes and all details in the geometry. By using symmetry of the real scale model, only one half of the structure appears in the mesh. In the critical areas (i.e. the high-gradient areas), the mesh quality has to be controlled, that is the aspect ratio of tetrahedrons should

be as close to 1 as possible in order to improve the FEM simulation's robustness. The mesh sizes near the air-gaps are set to depend directly on the corresponding air-gap thickness  $\epsilon$ , usually the characteristic length ranges from  $0.5\epsilon$  to  $1.5\epsilon$ . Since the tooth air-gap is really small compared to the global size of the model (0.1 mm compared to 150 mm) the mesh size is quite important:  $8.8 \cdot 10^6$  tetrahedrons.

The mesh is obtained through the software Gmsh [10] and Salome (Netgen algorithm). It can be noted that stator packets are meshed as a homogeneous block (treated as an anisotropic medium), allowing to greatly reduce the mesh size (and thus the needed memory and time for the creation of the stiffness matrix) at the cost of the resolution time (about 80 h of resolution).

### C. Anisotropy validation

Using anisotropic domains is a good way of modeling the stack of sheets. The anisotropy of the conductivity  $\sigma$  over the transverse direction of the stack in FEM simulations has been explored by Yamazaki et al. [11], along with other methods; but the relations involving the characteristics of the material (isotropic and anisotropic) in regard to the stacking factor have been given by Jackson [4] for example 35 years ago.

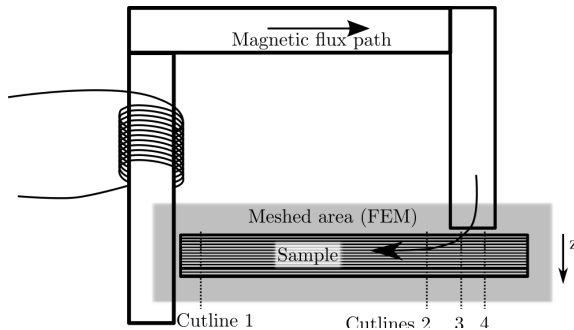


Figure 4. Basic apparatus used as simplified reference case.

The anisotropy on materials was investigated with code\_Carmel3D in previous works on a basic apparatus (see in figure 4) where the flux incomes transversely to the sheets and outcomes in the lamination direction. Experimental results will not be presented in this paper. The sample is made of 15 sheets (dimensions  $100 \times 30 \times 0.35$  mm) and the coating thickness is assumed to equals 0.015 mm (the stacking factor  $\gamma$  is therefore 0.955). Three models have been considered:

- 1) Each sheet and coating meshed with “one layer” (*i.e.* one layer of hexahedrons split into tetrahedrons: thus the elements barycenters are spread on three layers);
- 2) Each sheet meshed with “three layers” and each coating with “one layer” (please refer to the figure 5), 3 mesh layers in the sheet thickness provides a good representation of skin depth effects, therefore this case is taken as reference in this comparison;
- 3) The sheets and their coating meshed globally into an homogenized block.

The model 1 leads to an average mesh of 4 millions elements, the model 2 to 23 millions elements and the model 3 is much lighter with 0.5 million elements. Defining “thin insulators” (mesh surfaces where  $\vec{J} \cdot \vec{n} = 0$ ) to represent each sheet coating was considered at first, but this method still requires the permeability to be anisotropic and a finer mesh; thus it was rejected.

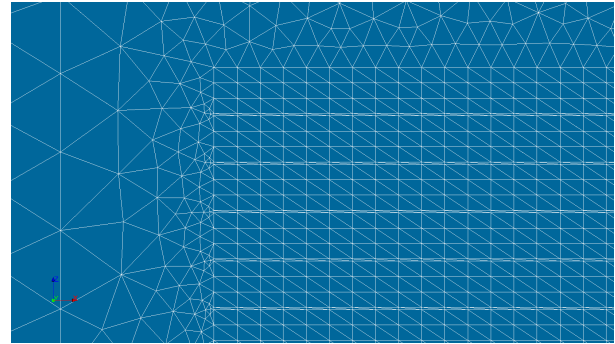


Figure 5. Mesh of the top end of the stack of sheets

Magnetic saturation is not considered. Both cases 1 and 2 are isotropic, and the model 3 uses anisotropic properties for the conductivity  $\sigma$  and the relative permeability  $\mu_r$ . They are roughly estimated:  $\sigma_t = 200 Sm^{-1}$  (compared to  $\sigma_l = 2.08 \cdot 10^6 Sm^{-1}$ ) and  $\mu_{r,t} = 22 = \frac{1}{1-\gamma}$  (compared to  $\mu_{r,l} = 3000$ ). The ratio between in plane and transverse values is really high, therefore these transverse parameters do not require an accurate gauging (their influence is low).

Finally, the results validate the use of anisotropy within code\_Carmel3D (see figure 6). The discretization introduces a “step” effect on the flux density along the cut lines that is particularly obvious in the case 3 since elements are much bigger; however the overall evolution and values are good. This simulation therefore confirms the modeling method of a stack of sheets by a homogenized anisotropic block.

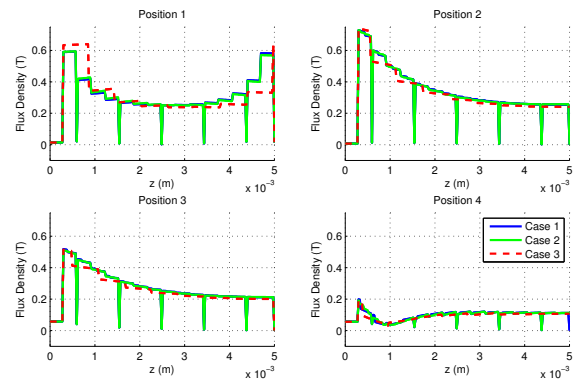


Figure 6. Flux density on cut-lines in the plane of symmetry (see figure 4). Cases 1 and 2 are really close (showing that one layer is enough), and 3 (dashed line) is a good approximation.

#### D. Losses analysis

1) *Loss density distribution*: Finite element analysis shows the distribution of loss density. In a first simulation, the current flowing through all the three windings are the same (phase and amplitude) and are set to induce in-phase fluxes in the tooth (therefore lengthwise and transverse excitation are in phase opposition in the exciter frames). On the figure 7 the loss density is drawn in this case.

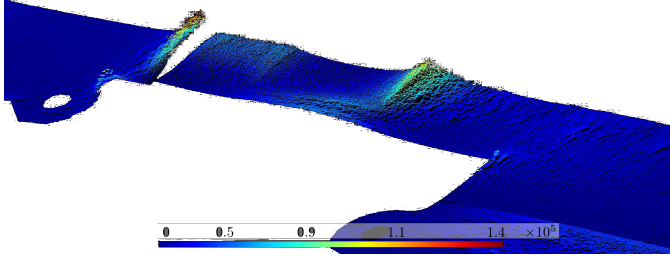


Figure 7. Loss repartition ( $W.m^3$ ) on the tooth. Only half of the device is drawn (the other half is symmetric).

The repartition of eddy current losses in tooth between the two transverse arms is quite even, while a higher loss density area appears “outside” (cf. figure 7). We can also notice that, as expected, the losses near the slot corner are high. Other plots (which are not drawn hereby) point out that losses are localized at the top of the sheet stack. With no doubt, taking into account the saturation phenomena would spread the losses into a larger area (deeper in the stack).

2) *Loss evolution with transverse flux amplitude*: The influence of transverse magnetic flux has been investigated: the lengthwise flux is fixed (5 A in both lengthwise windings) and the transverse flux varies, the evolution is presented in the figure 8. Positive values of current mean that transverse and lengthwise currents tends to create an in-phase flux in the tooth.

Since the transverse frame constitutes an acceptable path for the flux (as shown in the table I), some of the flux from lengthwise excitation is driven by the transverse frame. Therefore it is seen as an offset value; and thus the effect of positive transverse current is to counterbalance this flux: 5 A are needed to get an average flux density of 0 T in the transverse frame (see both x-axes in the figure 8).

### IV. LOSS MEASUREMENT

#### A. Protocol

Search coils have been implemented to measure the flux actually flowing in the iron close to the (B), (D) and (C') (end of the tooth) markers of the figure 2. The loss are measured with a precision wattmeter while fluxes are computed from search coils voltage waveforms. The use of search coils allows to subtract the losses from Joule's effect in the windings.

#### B. Influence of the transverse frame (passive)

The first result deals about the effect of the exciter frame itself. Both lengthwise windings (B) generate an in-phase flux

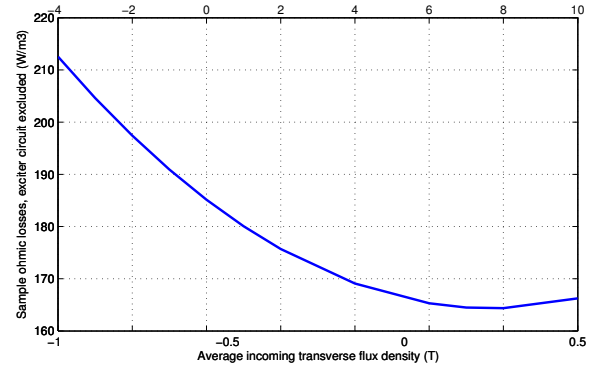


Figure 8. Influence of transverse flux amplitude: ohmic losses in the sample with respect to the average incoming transverse flux density. Upper x-axis shows the corresponding current set in the transverse winding.

in the tooth (up to  $1.8 T$ ). In the first case, the transverse frame is absent, and in the second case it is put in the position described in the figure 2 with no excitation. The overall flux path in the tooth is changed by the presence of the frame: around 5-8% of the flux (depending on the tooth saturation) flows through the transverse frame. This flux is therefore normal to the sheet planes and induces additional losses that are presented in the figure 9.

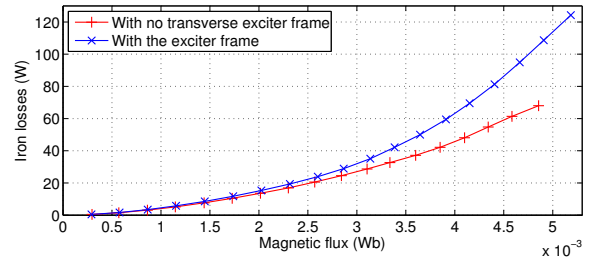


Figure 9. Iron losses seen from one lengthwise winding (B) function of the magnetic flux in one lengthwise arm.

#### C. Evaluation of tooth losses

In order to evaluate the losses within the tooth due to the transverse flux, several experiments are made:

- 1) The transverse frame is fully on the lengthwise exciter, fitting with the (F) marks (figure 2); the (B) windings are short-circuited whereas the (E) windings generates a magnetic flux.
- 2) Same as 1, but the (B) windings induce a high flux ( $3.8 mWb$  in each arm) in-phase in the tooth. In this case one arm of the transverse frame is upon a saturated area (near the tooth), so its behavior is the same as the basic case (shown in figure 2).
- 3) The transverse frame is absent, and the (B) windings induce the same flux as in 2.
- 4) Same as 2, but the transverse frame is in the position shown in the figure 2.

The losses within the tooth due to the transverse flux ( $T$ ) in the case 4 are therefore:

$$T_4 = P_4 - P_3 - (P_2 - \frac{1}{2}P_1)$$

where  $P_i$  are the total losses in the experiment  $i$  excepted in the case of  $P_2$  where only the losses seen from the transverse winding (D) are taken into account.

The additional losses due to the transverse field are presented in the figure 10. The flux flowing through the lengthwise arms remains constant, and the losses due to this lengthwise flux in the whole magnetic circuit are 78 W. Assuming that half of the losses are localized in the tooth, the additional losses under a 0.25 T transverse flux represents an increase of 12% of the losses.

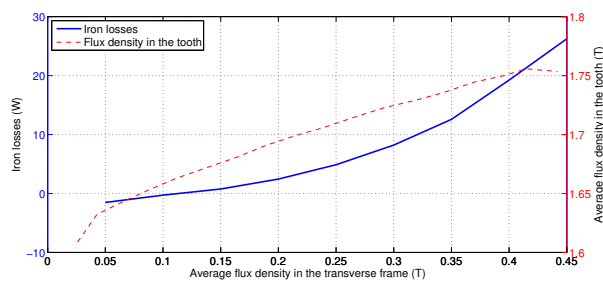


Figure 10. Additional losses in the tooth due to the transverse flux only.

## V. CONCLUSION

The experimental apparatus has been carefully presented: the methodology used for designing the device was explained with respect to the background and objectives, in a way intended to be systematic and pedagogic. A simple reluctance network was used to anticipate the global flux behavior (in regard to air-gaps notably) and to determine the windings characteristics (number of turns, current, voltage).

Finite elements analysis (3D) gives a finer idea of flux repartition, and in particular of ohmic losses. Moreover, as soon it will be calibrated with the experimental results (which are usually global or integrated physical quantities), it will provide accurate and local results.

Some results have been presented regarding the effect of the transverse flux on the tooth. First, a small part of the magnetic flux flowing through the tooth have been passively deflected by the transverse frame and lead to an important increase of losses. In a real alternator, this deviation embodies the air gap fringing for example. A second result deals with the localized increased of losses in the tooth as a function of the amplitude of the incoming transverse flux density. Based on the losses of four experimental setups, we have deduced the losses due to the axial flux only in the tooth.

In the future, more features could be added to the device, such as teeth slits; asymmetric lengthwise excitations may also be studied. Thin search coils will be added between laminations, and thermal measurement will be made with

an infrared camera. The transverse flux incoming area could be improved by covering a bigger area upon the tooth. Of course, the consideration of saturation would also ameliorate the accuracy of results, but at the cost of computing time and complexity of anisotropy. Nevertheless, simulations are ultimately meant to model the whole end region of a turbo-generator.

## ACKNOWLEDGMENT

This work is supported by MEDEE program supervised by the French national technological research cluster on electrical machine efficiency increase. This program that includes Électricité de France R&D is sponsored by the region Nord Pas-de-Calais (France) and the French ministry and the European funds (FEDER).

## REFERENCES

- [1] P. Drzymala, K. Komeza, H. Welfle, S. Wiak, D. Kardas, and S. Sieradzki, "Field analysis of end regions of stator windings of large turbo-generators," in *IEEF 2009 - XIV International Symposium on Electromagnetic Fields in Mechatronics, Electrical and Electronic Engineering*, 2009.
- [2] R. Lin, A. Haavisto, and A. Arkkio, "Analysis of eddy-current loss in end shield and frame of a large induction machine," *IEEE Transactions on Magnetics*, vol. 46, no. 3, pp. 942–948, 2010.
- [3] B. Mecrow, A. Jack, and C. Cross, "Electromagnetic design of turbogenerator stator end regions," *Generation, Transmission and Distribution, IEE Proceedings C*, vol. 136, no. 6, pp. 361–372, Nov. 1989.
- [4] R. Jackson, "Interlamination voltages in large turbogenerators," *Proceedings of the Institution of Electrical Engineers*, vol. 125, no. 11, pp. 1232–1238, 1978.
- [5] S. B. Lee, G. Kliman, M. Shah, W. Mall, N. Nair, and R. Lusted, "An advanced technique for detecting inter-laminar stator core faults in large electric machines," *Industry Applications, IEEE Transactions on*, vol. 41, no. 5, pp. 1185–1193, sept.-oct. 2005.
- [6] R. Singleton, P. Marshall, and J. Steel, "Axial magnetic flux in synchronous machines: The effect of operating conditions," *IEEE Transactions on Power Apparatus and Systems*, vol. PAS-100, no. 3, pp. 1226–1233, 1981.
- [7] R. Hilliar, R. Jackson, D. Ward, and R. Bennett, "Measurements of the currents flowing in the stator frame of a 500 mw turbogenerator," *Generation, Transmission and Distribution, IEE Proceedings C*, vol. 133, no. 1, pp. 16–25, 1986.
- [8] R. Platt, L. Kerr, and A. Anderson, "Measuring flux and interlaminar voltage in turbine generator end regions," in *IEE EMDA Conf., London*, vol. Conf. Pubn. 213, 1982, pp. 201–205.
- [9] V. Karapetoff, *The Magnetic Circuit - Electromagnetic Engineering*, M. Books, Ed. Watchmaker Publishing, 2003.
- [10] C. Geuzaine and J.-F. Remacle, "Gmsh: A 3-d finite element mesh generator with built-in pre- and post-processing facilities," *International Journal for Numerical Methods in Engineering*, vol. 79, no. 11, pp. 1309–1331, 2009. [Online]. Available: <http://doi.wiley.com/10.1002/nme.2579>
- [11] K. Yamazaki, S. Tada, H. Mogi, Y. Mishima, C. Kaido, S. Kanao, K. Takahashi, K. Ide, K. Hattori, and A. Nakahara, "Eddy current analysis considering lamination for stator core ends of turbine generators," *IEEE Transactions on Magnetics*, vol. 44, no. 6, pp. 1502–1505, 2008.